

UC Davis

UC Davis Previously Published Works

Title

Mechanism of microtubule lumen entry for the  $\alpha$ -tubulin acetyltransferase enzyme  $\alpha$ TAT1.

Permalink

<https://escholarship.org/uc/item/24s2602f>

Journal

Proceedings of the National Academy of Sciences of USA, 113(46)

Authors

Coombes, Courtney

Yamamoto, Ami

McClellan, Mark

et al.

Publication Date

2016-11-15

DOI

10.1073/pnas.1605397113

Peer reviewed

# Mechanism of microtubule lumen entry for the $\alpha$ -tubulin acetyltransferase enzyme $\alpha$ TAT1

Courtney Coombes<sup>a</sup>, Ami Yamamoto<sup>a</sup>, Mark McClellan<sup>a</sup>, Taylor A. Reid<sup>a</sup>, Melissa Plooster<sup>a</sup>, G. W. Gant Luxton<sup>a</sup>, Joshua Alper<sup>b</sup>, Jonathon Howard<sup>c</sup>, and Melissa K. Gardner<sup>a,1</sup>

<sup>a</sup>Department of Genetics, Cell Biology, and Development, University of Minnesota, Minneapolis, MN 55455; <sup>b</sup>Department of Physics and Astronomy, Clemson University, Clemson, SC 29634; and <sup>c</sup>Department of Molecular Biophysics and Biochemistry, Yale University, New Haven, CT 06520

Edited by Eva Nogales, University of California, Berkeley, CA, and approved October 5, 2016 (received for review April 3, 2016)

**Microtubules are structural polymers inside of cells that are subject to posttranslational modifications. These posttranslational modifications create functionally distinct subsets of microtubule networks in the cell, and acetylation is the only modification that takes place in the hollow lumen of the microtubule. Although it is known that the  $\alpha$ -tubulin acetyltransferase ( $\alpha$ TAT1) is the primary enzyme responsible for microtubule acetylation, the mechanism for how  $\alpha$ TAT1 enters the microtubule lumen to access its acetylation sites is not well understood. By performing biochemical assays, fluorescence and electron microscopy experiments, and computational simulations, we found that  $\alpha$ TAT1 enters the microtubule lumen through the microtubule ends, and through bends or breaks in the lattice. Thus, microtubule structure is an important determinant in the acetylation process. In addition, once  $\alpha$ TAT1 enters the microtubule lumen, the mobility of  $\alpha$ TAT1 within the lumen is controlled by the affinity of  $\alpha$ TAT1 for its acetylation sites, due to the rapid rebinding of  $\alpha$ TAT1 onto highly concentrated  $\alpha$ -tubulin acetylation sites. These results have important implications for how acetylation could gradually accumulate on stable subsets of microtubules inside of the cell.**

microtubule | acetylation | biophysics | microscopy | modeling

**M**icrotubules are dynamic structural polymers that participate in cell and organelle morphology and motility, intracellular transport, signaling, and chromosome movement during mitosis. Despite these various roles, microtubule structure is highly conserved: microtubules across a wide range of organisms are hollow tube structures that are made up of  $\alpha$ - and  $\beta$ -tubulin heterodimers stacked end-to-end into protofilaments. For microtubules to perform such a wide range of tasks, the cell uses a variety of posttranslational modifications to fine-tune their function (1, 2). Unlike the other known microtubule posttranslational modifications, the enzyme responsible for microtubule acetylation must access the  $\alpha$ -tubulin Lysine 40 (Lys40) site inside the hollow portion of the microtubule, known as the lumen, to acetylate microtubules (3, 4). Because of this unique localization to the lumen, the functional consequences of microtubule acetylation were initially puzzling to the field. However, recent functional studies have revealed effects of microtubule acetylation on cell signaling (5), cell cycle progression (6), and breast cancer cell migration (7). In humans, microtubule acetylation may be important for intracellular cargo transport in neurons and neuronal maintenance in neurodegenerative disease contexts, including Alzheimer's (8), Parkinson's (9, 10), and Huntington's (11) diseases.

The primary enzyme that is responsible for  $\alpha$ -tubulin Lys40 acetylation in mammals, nematodes, and protozoa has been identified as  $\alpha$ -tubulin acetyltransferase 1 ( $\alpha$ TAT1), which was first found in *Tetrahymena* and *Caenorhabditis elegans* (12–14). However, despite identification of the enzyme and its substrate, the mechanism for how  $\alpha$ TAT1 enters the microtubule lumen to access its acetylation sites is yet to be fully understood. There are several potential mechanisms for how  $\alpha$ TAT1 may access the acetylation site on the inside of the microtubule lumen: by copolymerization with tubulin at growing microtubule plus-ends (15), by transient openings in the lattice during microtubule breathing

(13, 16, 17), or by microtubule end-entry (12, 18). Copolymerization is not likely to be the primary mechanism for  $\alpha$ TAT1 access, because stable microtubules are acetylated, and because  $\alpha$ TAT1 is more active on polymerized microtubules than on free tubulin dimers (12, 13, 19–25). Conversely, the other modes of access are possible (12, 13, 18). Distinguishing among these possibilities is important for developing a mechanistic understanding to explain how  $\alpha$ TAT1 could access its acetylation sites to facilitate microtubule acetylation.

In this work, we found that  $\alpha$ TAT1 enters the microtubule lumen from the microtubule ends, and through breaks and bends in the lattice. Further, recent work suggested that  $\alpha$ TAT1 was able to diffuse efficiently within the microtubule lumen, and thus acetylate microtubules without a preference for microtubule ends (18). However, our results support a model in which the mobility of  $\alpha$ TAT1 within the lumen is controlled by the affinity of  $\alpha$ TAT1 for its acetylation sites, which are highly concentrated inside of the microtubule lumen, and in which the acetylation efficiency of  $\alpha$ TAT1 is regulated, in part, by the accessibility of acetylation sites through alterations in microtubule structure.

## Results

**$\alpha$ TAT1 Is Concentrated Near to Microtubule Ends.** To investigate the localization of  $\alpha$ TAT1 binding to the microtubule, we used total internal reflection fluorescence (TIRF) microscopy to visualize the interactions of purified  $\alpha$ TAT1-GFP protein (*SI Appendix, Fig. S1A*) with guanosine-5'-[( $\alpha,\beta$ )-methylene]triphosphate (GMPCPP)-stabilized (nondynamic), rhodamine-labeled microtubules (13). Here, purified tubulin was combined with the slowly hydrolyzable GTP analog, GMPCPP, and incubated for 2 h. The resulting

## Significance

**$\alpha$ TAT1 is an enzyme that acetylates microtubules inside of cells, and acetylation is an important posttranslational microtubule modification. However, microtubules are long tubes, and the acetylation site for  $\alpha$ TAT1 is on the inside of this tube. We investigated how  $\alpha$ TAT1 enters the microtubule and moves around to access its acetylation sites once inside. We found that  $\alpha$ TAT1 enters microtubules through its ends but does not move efficiently inside of the microtubule. However, a lowered affinity allows the enzyme to move more efficiently and leads to longer stretches of acetylation. Therefore, acetylation of microtubules could be controlled in the cell by modulating the affinity of  $\alpha$ TAT1 for its acetylation site or increasing the number of microtubule ends.**

Author contributions: C.C., M.M., G.W.G.L., J.A., J.H., and M.K.G. designed research; C.C., A.Y., M.M., and M.P. performed research; M.M., T.A.R., and M.K.G. contributed new reagents/analytic tools; C.C., A.Y., M.M., and M.K.G. analyzed data; and C.C. and M.K.G. wrote the paper.

The authors declare no conflict of interest.

This article is a PNAS Direct Submission.

<sup>1</sup>To whom correspondence should be addressed. Email: klei0091@umn.edu.

This article contains supporting information online at [www.pnas.org/lookup/suppl/doi:10.1073/pnas.1605397113/-DCSupplemental](http://www.pnas.org/lookup/suppl/doi:10.1073/pnas.1605397113/-DCSupplemental).

microtubules were then attached to a coverslip in an imaging chamber using antirhodamine antibody, and 30 nM  $\alpha$ TAT1-GFP (*SI Appendix, Fig. S1 A and C*) in imaging buffer was then introduced to the imaging chamber (*SI Appendix*). After steady-state binding was achieved ( $\sim 20$  min; *SI Appendix, Fig. S1B*), single-time-point images were collected using TIRF microscopy (*Fig. 1A*). Qualitatively, we observed that  $\alpha$ TAT1-GFP was concentrated near to the microtubule ends (*Fig. 1B, Top*; typical images). We then quantified the microtubule images, and the corresponding green  $\alpha$ TAT1-GFP fluorescence, by plotting the average red tubulin and green  $\alpha$ TAT1-GFP fluorescence intensity as a function of the distance from the highest red fluorescence intensity (bright) microtubule end to the lowest red fluorescence intensity (dim) microtubule end [*Fig. 1B, Bottom* (red, microtubule; gray,  $\alpha$ TAT1-GFP) and *SI Appendix, Fig. S2A*]. Here, the “dim” end of the microtubule is likely composed of variable protofilament lengths (26–28), and thus may expose the internal microtubule luminal surface (*Fig. 1B, cartoon*), an effect that may be enhanced by the microtubule depolymerizing properties of  $\alpha$ TAT1 (29) (*SI Appendix, Fig. S2C*). We then normalized the green  $\alpha$ TAT1-GFP fluorescence intensity to its

corresponding red microtubule fluorescence intensity at each microtubule position (*Fig. 1B, Bottom*; green markers) to account for reduced total tubulin polymer at the dim microtubule end. We found that the normalized  $\alpha$ TAT1-GFP concentration was higher at microtubule ends, and especially on the dim end of the microtubule, which suggests that  $\alpha$ TAT1 is concentrated on exposed luminal sites at open, tapered microtubule ends (*Fig. 1B and SI Appendix, Fig. S2*). To test whether less tapered, “blunt” microtubule tips had reduced targeting of  $\alpha$ TAT1-GFP to their ends, we generated a new population of microtubules that were grown for a shorter amount of time ( $\sim 10$  min), which allowed us to analyze microtubules with reduced taper at the microtubule end (*SI Appendix, Fig. S2B*). Consistent with the idea that open, tapered microtubule ends with exposed acetylation sites more readily bind  $\alpha$ TAT1 as compared to closed, blunt ends, we observed reduced targeting of  $\alpha$ TAT1-GFP on the blunt microtubule tips (*SI Appendix, Fig. S2B*).

To confirm that  $\alpha$ TAT1 binding was concentrated in areas of the microtubule with exposed luminal sites, we conjugated purified, unlabeled  $\alpha$ TAT1 (*SI Appendix, Fig. S1A*) to 1.3-nm-diameter gold beads, incubated the  $\alpha$ TAT1-conjugated beads with GMPCPP-stabilized microtubules for 20 min, and then imaged the microtubules using transmission electron microscopy (TEM) (*SI Appendix*). The 1.3-nm-diameter beads act as reporters for  $\alpha$ TAT1 localization, but they should not limit access to the lumen because they are smaller than the inner diameter of the microtubule ( $\sim 15$  nm). Consistent with the  $\alpha$ TAT1-GFP fluorescence data, 86% of the observed  $\alpha$ TAT1-conjugated bead clusters were located either at open microtubule ends or at breaks or openings in the lattice (*Fig. 1C, Top*; red arrows and bars). This result is in contrast to BSA-conjugated control beads, in which 83% of BSA beads did not bind microtubules at all (*Fig. 1C, Middle*; black *Inset*), and of the remainder of the BSA beads, 13% were bound to the lattice and 4% to microtubule ends. For a positive control, we then conjugated monomeric (truncated) kinesin-1 to beads, mixed the kinesin beads with microtubules in the presence of adenylyl-imidodiphosphate (AMPPNP) to allow for rigor binding, and then imaged the kinesin beads and microtubules using TEM (30) (*Fig. 1C, Middle*; blue arrow and bar). We then directly compared the localization of the  $\alpha$ TAT1-conjugated beads with the stationary kinesin-conjugated beads (*Fig. 1C, Bottom*), and found that although 86% of the bound  $\alpha$ TAT1 beads were at microtubule tips or defects, only 15% of the kinesin beads were at tips or defects, with the remainder of the kinesin beads (85%) bound to the closed lattice (*Fig. 1C*). This finding suggests that  $\alpha$ TAT1 specifically targeted the beads to open microtubule ends and lattice openings.

**Simulations Suggest  $\alpha$ TAT1-GFP End-Entry into the Microtubule Lumen.** To investigate whether the experimentally observed  $\alpha$ TAT1-GFP localization on stabilized microtubules could correlate with a lumen entry mechanism, we performed computational simulations of the  $\alpha$ TAT1–microtubule interaction. Our simulations accounted for the (i) association and dissociation of  $\alpha$ TAT1 with tubulin subunits on the external surface of the lattice, and diffusion of  $\alpha$ TAT1 on this surface (*Fig. 2A, Left*; *SI Appendix*; and *SI Appendix, Fig. S3*), (ii) association and dissociation of  $\alpha$ TAT1 on the internal luminal surface of the microtubule and diffusion in solution within the lumen (*Fig. 2A, Center*), and (iii) adjusting of the simulated microtubule tip structures to match experimentally observed average microtubule-associated fluorescence lines scans (*Fig. 2A, Right*). We constrained our model parameters either through experiments (*SI Appendix, Fig. S3*), or, alternatively, by testing them over a range of values to ensure that model conclusions did not depend on narrowly defined parameter values (*SI Appendix, Fig. S3*). We found that the modeling results for  $\alpha$ TAT1-GFP localization on microtubules were most sensitive to the parameter  $\gamma$ , which controls the  $\alpha$ TAT1 off-rate (affinity) on the luminal surface of the microtubule, as described below.

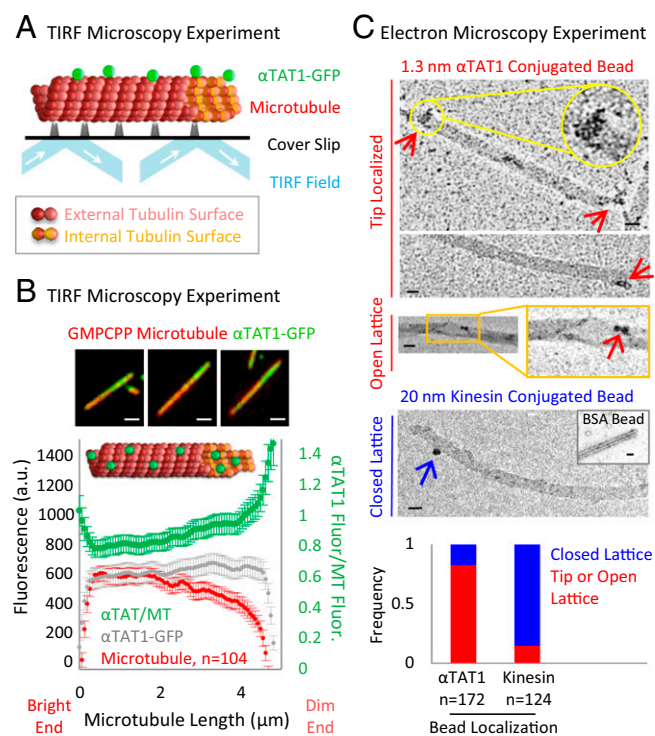


**Fig. 1.**  $\alpha$ TAT1 preferentially targets the dim microtubule ends of GMPCPP-stabilized microtubules. (A) TIRF microscopy experiments to characterize  $\alpha$ TAT1-GFP localization (green) on microtubules (red). (B, Top) Typical images of  $\alpha$ TAT1-GFP binding (green) to rhodamine-labeled GMPCPP microtubules (red). (Scale bars: 1  $\mu\text{m}$ .) (B, Bottom) Quantitative average fluorescence line scans indicating the localization of  $\alpha$ TAT1-GFP on microtubules [ $n = 104$  microtubules, error bars illustrate 95% confidence intervals, and green markers are  $\alpha$ TAT-GFP intensity (gray) normalized to microtubule intensity (red) at each position]. Data from other microtubule lengths are shown in *SI Appendix, Fig. S1C*. (*Inset*) Cartoon demonstrates the preferential localization of  $\alpha$ TAT1-GFP to the dim microtubule end. (C, Top) TEM images of  $\alpha$ TAT1 conjugated to a 1.3-nm gold bead (red arrows point to  $\alpha$ TAT bead clusters at tips and open microtubule lattice). (C, Middle) TEM images of monomeric kinesin-1 conjugated to a 20-nm gold bead (blue arrow points to a kinesin bead on the microtubule lattice). (*Inset*) BSA conjugated to 1.3-nm gold beads with stabilized GMPCPP microtubules. (Scale bars: 25 nm.) (C, Bottom) Quantification for localization of  $\alpha$ TAT1 beads compared with kinesin beads. au, arbitrary units; Fluor, fluorescence; MT, microtubule.

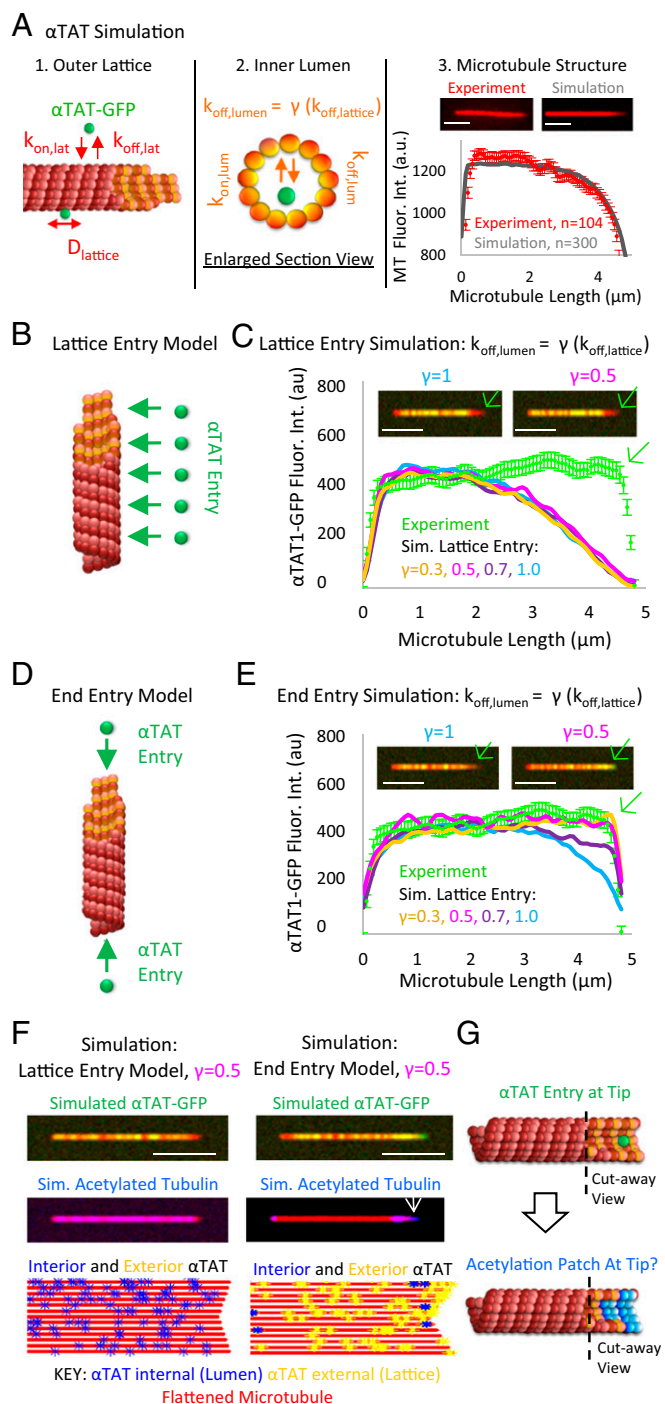


**Fig. 2.** Simulations predict differential acetylation patterns based on the  $\alpha$ TAT1 microtubule entry model. (A) Rules for  $\alpha$ TAT1 simulation, which include (i) movement and binding of  $\alpha$ TAT1 on the external surface of the microtubule (Left), (ii) binding and unbinding of  $\alpha$ TAT1 on the inside surface of the microtubule (Center), and (iii) adjusting of simulated microtubule (MT) tip structure to match experimental fluorescence line scale profiles (Right). (B) In the simulated  $\alpha$ TAT1 lattice entry model,  $\alpha$ TAT1 is able to enter the lumen randomly at any point along the microtubule. (C) Lattice-entry model does not reproduce experimental  $\alpha$ TAT1-GFP localization results, regardless of the value for  $\gamma$ . (D) In the simulated  $\alpha$ TAT1 end-entry model,  $\alpha$ TAT1 is only able to enter the microtubule lumen from its ends. (E) End-entry model reproduces experimental  $\alpha$ TAT1-GFP localization results if  $\gamma \leq 0.5$ . (F) Simulated  $\alpha$ TAT1-GFP localization (Top), the resulting distribution of acetylated tubulin (Middle), and a cartoon of resulting locations of simulated  $\alpha$ TAT1 molecules (Bottom), when using the lattice entry model (Left) and end entry model (Right) (also *Movies S1* and *S2*). (G) Luminal  $\alpha$ TAT1 (green) diffuses in solution

We then used the simulation to predict  $\alpha$ TAT1-GFP localization for two potential models that explain how  $\alpha$ TAT1 could enter into the microtubule (end vs. lattice entry). We first tested a microtubule “lattice entry” model in which simulated  $\alpha$ TAT1 could bind the microtubule lattice, and then subsequently enter into the lumen regardless of its position along the microtubule (Fig. 2B), similar to a “breathing” model in which transient lattice openings could routinely provide access for  $\alpha$ TAT1 to enter the lumen along the length of the lattice. Using the lattice entry model, the simulated  $\alpha$ TAT1-GFP localization data were not consistent with the experimentally observed localization of  $\alpha$ TAT1-GFP at the microtubule tip (Fig. 2C). We ran this simulation for multiple values of  $\gamma$ , which is the relative affinity of  $\alpha$ TAT1 for  $\alpha$ -tubulin Lys40 acetylation sites on the inside surface versus the outside of the microtubule [ $k_{off,lumen} = \gamma(k_{off,lattice})$ ]. We found that the lattice entry model failed to explain the experimental data, regardless of the value for  $\gamma$  (Fig. 2C).

Next, we used our simulations to test a microtubule “end-entry” model, in which simulated  $\alpha$ TAT1 could only enter the lumen through the microtubule ends (Fig. 2D). The simulated  $\alpha$ TAT1-GFP localization data were consistent with the experimentally observed localization of  $\alpha$ TAT1-GFP at the microtubule tip for  $\gamma \leq 0.5$  ( $k_{off,lumen} = 0.5$  per second; Fig. 2E), meaning that the simulated localization of  $\alpha$ TAT1-GFP on stabilized microtubules was consistent with the experiment if (i)  $\alpha$ TAT1 entered the lumen at microtubule ends and (ii) the simulated off-rate of  $\alpha$ TAT1 was twofold higher on the outside of the lattice relative to its acetylation site on the luminal surface of the microtubule (i.e.,  $k_{off,lumen} = 0.5$  per second).

Thus, the results from these simulations suggest that the primary mode of  $\alpha$ TAT1 entry into the lumen is through the microtubule ends, and that the affinity of  $\alpha$ TAT1 for the  $\alpha$ -tubulin Lys40 acetylation sites within the lumen is higher than its affinity for the outside of the microtubule. However, our  $\alpha$ TAT1-GFP localization studies could not differentiate whether the experimentally observed  $\alpha$ TAT1-GFP molecules were on the inside or the outside of the microtubule (Fig. 1B). Therefore, we used the simulation to predict the pattern of acetylation on the inside of a stabilized microtubule, as would be visualized using a fluorescent antiacetylated tubulin antibody. We found that the lattice-entry model predicted uniformly distributed acetylated tubulin subunits along the length of the microtubule (Fig. 2F, *Left Middle* and *Movie S1*) because the  $\alpha$ TAT1 molecules that entered the lumen along the length of the microtubule lattice were randomly localized along the inside of the microtubule (Fig. 2F, *Left Bottom*; cartoon). Conversely, we found that the end-entry simulation predicted concentrated, short “patches” of acetylation at microtubule ends (Fig. 2F, *Right Middle* and *Movie S2*). These patches were predicted because the  $\alpha$ TAT1 molecules that entered the lumen through the microtubule ends tended to remain near to the microtubule ends (Fig. 2F, *Right Bottom*; cartoon).

In the end-entry  $\alpha$ TAT1 simulation, the luminal  $\alpha$ TAT1 molecules remained near to the microtubule ends because the simulated  $\alpha$ TAT1 molecules exhibited very slow mobility inside of the microtubule lumen. Although it is expected that  $\alpha$ TAT1 should diffuse rapidly in solution within the lumen, the concentration of  $\alpha$ -tubulin Lys40 binding sites inside of the lumen is very high due to the small volume and dense packing of tubulin subunits inside the lumen ( $\sim 17$  mM; calculated in *SI Appendix*). This high concentration of  $\alpha$ -tubulin Lys40 binding sites within the lumen makes the effective on-rate for an individual  $\alpha$ TAT1 molecule inside of a microtubule also very high. For example, we predict that the typical rebinding time for a free  $\alpha$ TAT1 molecule inside the lumen will be

but rapidly rebinds to nearby tubulin subunits. (Top) Thus,  $\alpha$ TAT1 moves slowly down the lumen. (Bottom) As a result, the simulation predicts patches of acetylated tubulin near to the microtubule end (blue, acetylated subunits) (Scale bars: 3  $\mu$ m.) Int., intensity; Sim., simulated.

$(1/(k_{on}[\text{binding sites}])) = 6 \times 10^{-5}$  per second (using a diffusion-limited biomolecular on-rate constant of  $k_{on} = 1 \mu\text{M}^{-1}\cdot\text{s}^{-1}$ ) (31). As a result, we further predict that the root mean squared travel distance for a free  $\alpha\text{TAT1}$  molecule before rebinding to an  $\alpha$ -tubulin Lys40 acetylation site ( $\Delta x_{lumen}$ ) would be  $\sim 50$  nm, where

$$\langle \Delta x_{lumen}^2 \rangle^{1/2} = \sqrt{2D_{lumen}\Delta t_{rebind}}, \quad [1]$$

in which  $D_{lumen}$  is the  $\alpha\text{TAT1}$  diffusion coefficient in solution ( $\sim 2.6 \times 10^7 \text{ nm}^2\cdot\text{s}^{-1}$ ) (18) and  $\Delta t_{rebind}$  is the typical rebinding time, as calculated above ( $\sim 6 \times 10^{-5} \text{ s}^{-1}$ ). This predicted mean travel distance is similar to previous computational predictions (32).

Thus, the end-entry model for  $\alpha\text{TAT1}$  predicts that there will be patches of acetylated tubulin near to the  $\alpha\text{TAT1}$  entry point at microtubule ends because the mobility of  $\alpha\text{TAT1}$  within the lumen may be limited by rapid rebinding of luminal  $\alpha\text{TAT1}$  to nearby tubulin subunits (Fig. 2G), with patch length further limited by a slow luminal off-rate (SI Appendix, Fig. S3C; simulated  $k_{off,lumen} = 0.5$  per second). This behavior led to two key predictions from the simulation that could be tested experimentally. First, if the end-entry model is correct, then acetylation should be most commonly observed near to the ends of the microtubules, where  $\alpha\text{TAT1}$  routinely enters the lumen. Second, if there is slow mobility of  $\alpha\text{TAT1}$  inside of the microtubule lumen due to rapid rebinding, then concentrated patches of microtubule acetylation should be observed, rather than a uniform dispersion of acetylation along the length of the microtubule (Fig. 2G).

**Microtubule Acetylation Occurs in Patches at Microtubule Ends.** We experimentally tested these simulation predictions by visualizing fluorescently labeled antiacetylated tubulin antibodies on rhodamine-labeled, GMPCPP-stabilized microtubules. Here, GMPCPP-stabilized microtubules were adhered to flow chamber coverslips as described above. A mixture of  $2.5 \mu\text{M}$  unlabeled  $\alpha\text{TAT1}$ ,  $2 \text{ mM}$  acetyl CoA (AcCoA), and Brb80 was then introduced into the imaging chamber and incubated with the coverslip-adhered microtubules for 30 min (Fig. 3A, Left). Then, the  $\alpha\text{TAT1}$  mixture was gently flushed from the chamber, and imaging buffer with CF488-labeled antiacetylated tubulin antibody was introduced to the chamber. The fluorescent antiacetylated tubulin antibody and microtubules were then imaged using TIRF microscopy (Fig. 3A, Left and Materials and Methods). We observed acetylation patches at the ends of microtubules (Fig. 3A, Right Top), similar to the simulation predictions for the end-entry model (Fig. 2F, Right; white arrow). The patches, which were defined as an area of fluorescent antibody localization along the length of the microtubule lattice, averaged  $\sim 300$  nm in length. This length represents up to  $\sim 200$  acetylated tubulin subunits [ $= ((300 \text{ nm} - 170 \text{ nm point spread function})/(8 \text{ nm/layer})) * (13 \text{ subunits/layer})$ ]. Less frequently, we also observed patches within the microtubule lattice (Fig. 3A, Right Bottom). To quantify this observation, we calculated the patch frequency per site by normalizing the patch frequency to the number of available sites in each case, where end sites represented the last 128 nm (two pixels) of a microtubule at each end and lattice sites represented the remainder of the microtubule. Similar to the predictions from our simulation, we found that patches were 15-fold more likely to occupy microtubule end sites than microtubule lattice sites (Fig. 3B; binomial test,  $P < 2 \times 10^{-6}$ ). Further, we measured the fluorescence intensity of the microtubule lattice at internal acetylation spots, and, consistent with the idea that internal acetylation may be correlated with broken microtubules, defects, or distinct microtubule ends, internal patches of acetylation were more frequently localized to dim areas on the microtubule compared with the mean microtubule brightness (Fig. 3B, Inset; binomial test,  $P = 3.4 \times 10^{-5}$ ).

To ensure that the antibody itself was not limited in its mobility to travel within the lumen, leading to an inability to detect

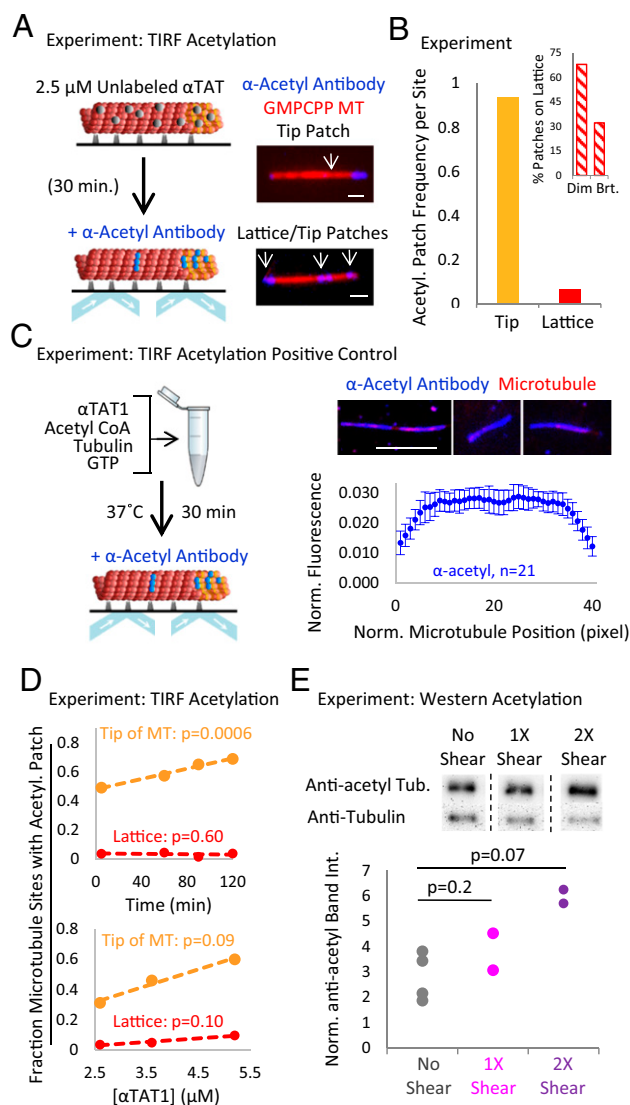


**Fig. 3.** Acetylation occurs in patches, which are preferentially localized at microtubule ends. (A, Left) Schematic of acetylation TIRF experiment. (A, Right) Typical images of acetylated microtubules. (Scale bars:  $1 \mu\text{m}$ .) (B) Patch frequency per site ( $n = 426$  microtubules). (Inset) Acetylation patches within the lattice were more likely to occur on dim areas of the microtubule. (C, Left) Schematic of positive control assay. (C, Right Top) Typical images of fully acetylated microtubules. (Scale bar:  $3 \mu\text{m}$ .) (C, Right Bottom) Quantification of average  $\alpha$ -acetyl antibody fluorescence along the length of fully acetylated microtubules of similar length. (D) Acetylation patch frequency by location on preformed, stabilized microtubules with increasing amounts of  $\alpha\text{TAT1}$  incubation time ( $2.5 \mu\text{M}$   $\alpha\text{TAT1}$ , Top) or increasing concentrations of  $\alpha\text{TAT1}$  ( $30$  min of  $\alpha\text{TAT1}$  incubation time, Bottom). To maintain consistency, the preparation of microtubules was held common within each of the experiments that measured acetylation with increasing time or concentration. (E) Results for microtubule shearing experiment as measured with Western blots. (Error bars in all panels are 95% confidence intervals, and  $P$  values are shown for comparison with same time point unsheared controls in each case). Acetyl., acetylated; Brt, bright; Norm., normalized; Tub, tubulin.

acetylation along the length of the microtubules, we performed a positive control experiment. Here, dynamic microtubules were grown in the presence of  $\alpha\text{TAT1}$  and AcCoA, in contrast to the stabilized microtubule experiments above, in which  $\alpha\text{TAT1}$  and AcCoA were added to preformed microtubules (Fig. 3C, Left vs. Fig. 3A). After 30 min of growth and acetylation, the dynamic microtubules were then stabilized with Taxol, introduced to an

imaging chamber, and imaged with the fluorescent antiacetylated tubulin antibody (Fig. 3C, *Left*). We observed a population of microtubules that were uniformly labeled with antibody over their entire lengths (Fig. 3C, *Right Top*), indicating that the antibody was indeed able to access a uniform proportion of the acetylated sites in the microtubules. To quantify this observation, average line scans for similar length, fully acetylated microtubules in the positive controls were collected. We found that the antibody brightness was uniform along the length of the microtubule for the fully acetylated controls (Fig. 3C, *Right Bottom*), indicating that the fluorescent antibody brightness as visualized by TIRF microscopy was similar whether the antibody reported acetylated tubulin subunits near to the ends of the microtubules or inside of the lumen along the length of the microtubule.

**Acetylation at Microtubule Ends Increases over Time.** To test whether increased  $\alpha$ TAT1 incubation time would increase the frequency of the acetylation patches, we incubated stable, preformed microtubules with 2.5  $\mu$ M  $\alpha$ TAT1 for times ranging from 5 to 120 min and then visualized microtubule acetylation with fluorescent antiacetylation antibody. We found that the fraction of microtubules with acetylation patches at their ends increased over time (Fig. 3D, *Top* and *SI Appendix, Fig. S4B*), and we note that a similar trend was observed with increasing  $\alpha$ TAT1 concentrations in which incubation time was held constant at 30 min (Fig. 3D, *Bottom* and *SI Appendix, Fig. S4A*). Thus, increasing the  $\alpha$ TAT1 incubation time (Fig. 3D, *Top*) or concentration (Fig. 3D, *Bottom*) led to a higher overall acetylation level due, in part, to an increased fraction of acetylated microtubule ends, consistent with an end-entry model. As indicated by the nonzero intercept in the frequency graphs in Fig. 3D (*Top*), we noted that a fraction of the microtubules displayed acetylation patches at their ends very quickly, followed by a slower increase over time for the remainder of the microtubules ( $P = 0.0006$ , linear regression). We hypothesize that the fraction of microtubule ends that were very quickly acetylated had readily accessible acetylation sites (e.g., via open, tapered ends), whereas the more slowly acetylated ends required rate-limiting entry of  $\alpha$ TAT1 into the microtubule through blunt ends, consistent with our observation that tapered microtubule ends have increased targeting of  $\alpha$ TAT1-GFP relative to blunt ends (Fig. 1B vs. *SI Appendix, Fig. S2B*).

If higher acetylation levels over time were due, in part, to an increased number of acetylated microtubule ends, and particularly to an increased number of tapered or opened microtubule ends, we reasoned that bulk acetylation levels would increase if the number of microtubule ends and/or lattice openings were increased by mechanical shearing and breaking of the microtubules. To test this prediction, we mixed rhodamine-labeled, GMPCPP-stabilized microtubules with unlabeled  $\alpha$ TAT1, separated half of the mixture, and sheared it using a small-diameter needle (1 $\times$  shear). After a 120-min incubation time, we sheared a portion of the 1 $\times$  mixture a second time (2 $\times$  shear), and then allowed the 2 $\times$  shear mixture to incubate for an additional 60 min. We quantified the acetylation levels for both mixtures using western blots, and then normalized each antiacetylation band intensity to its tubulin loading control to account for loss of microtubules inside of the syringe during the shearing process (Fig. 3E, *Top*). We found that the microtubule acetylation levels were slightly higher for the 1 $\times$  sheared mixture relative to its nonsheared control ( $P = 0.2$ ) and that the 2 $\times$  sheared mixture was substantially more acetylated than its unsheared control ( $P = 0.07$ ; Fig. 3E, *Bottom*). This finding suggests that the microtubules were broken into smaller fragments and/or damaged by successive cycles of shearing, which generated new microtubule ends and/or openings in the lattice during each cycle, and thus allowed for more acetylated microtubule ends and/or lattice openings. The increase in acetylated microtubule ends then led to a higher bulk acetylation level (16). Thus, microtubule acetylation may be facilitated by increased numbers of microtubule ends or new lattice openings.

**Microtubule Acetylation Is Facilitated by New Lattice Openings.** In addition to mechanical shearing, another method for allowing access of  $\alpha$ TAT1 to the microtubule lumen may be by introducing large breaks or openings within the microtubule wall (Fig. 4A). Thus, we predicted that by opening up the closed tube, or by introducing breaks into the tube, increased numbers of acetylation patches would be observed along the length of the microtubule lattice, and there would be an increase in the bulk acetylation level of a microtubule population (Fig. 4B).

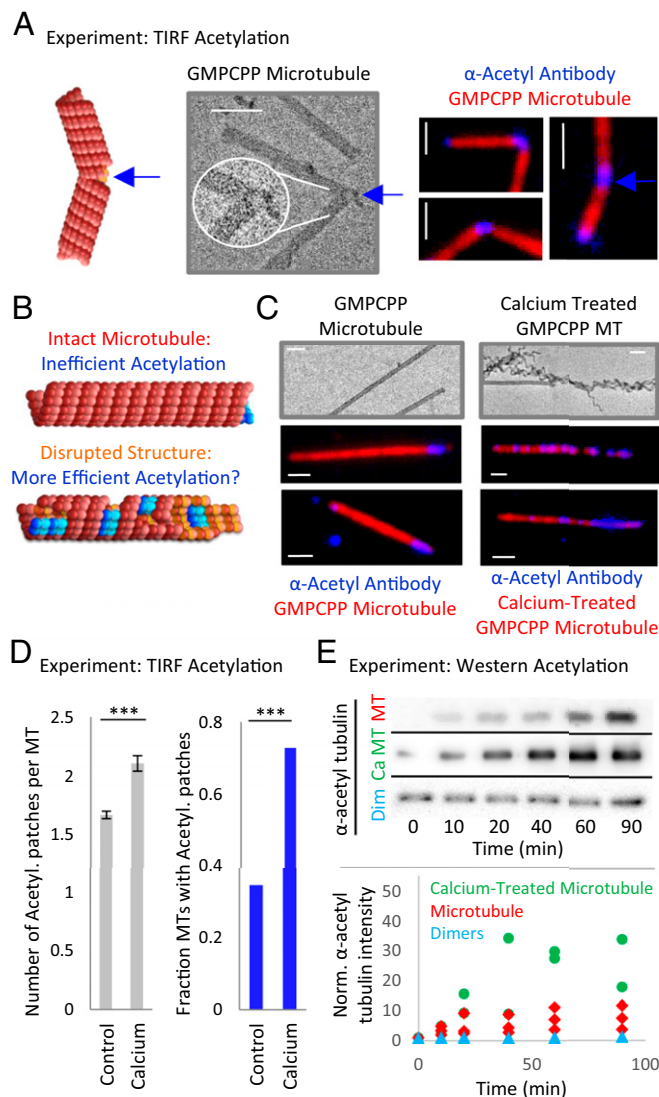


**Fig. 4.** Disruption of microtubule structure is correlated with higher acetylation rates. (A, *Left*) Schematic and TEM image of microtubule break at a bend. (Scale bar: 100 nm.) (A, *Right*) Acetylation-TIRF microscopy images of bent microtubules. (Scale bars: 1  $\mu$ m.) (B) If  $\alpha$ TAT1 typically enters the microtubule through its ends (*Top*), then the presence of new openings in the lattice may increase the acetylation rate (*Bottom*) (C, *Top*) TEM images of GMPCPP microtubules (*Left*), and  $\text{CaCl}_2$ -treated GMPCPP microtubules (*Right*). (Scale bars: 100 nm.) (C, *Middle and Bottom*) TIRF microscopy images of acetylated GMPCPP and  $\text{CaCl}_2$ -treated GMPCPP microtubules. (Scale bars: 1  $\mu$ m.) (D, *Left*) Mean number of patches per microtubule in control vs.  $\text{CaCl}_2$ -treated microtubules (control:  $n = 3,533$ , SD = 0.98;  $\text{CaCl}_2$ :  $n = 2,540$ , SD = 1.46).  $***P < 2 \times 10^{-6}$ . (D, *Right*) Fraction of microtubules that had at least one patch (control:  $n = 3,533$ ,  $\text{CaCl}_2$ :  $n = 2,540$ ). (E, *Top*) Representative western blots of acetylated dimers, GMPCPP microtubules, and  $\text{CaCl}_2$ -treated GMPCPP microtubules taken after 0–90 min of  $\alpha$ TAT1 incubation (also *SI Appendix, Fig. S4E*). (E, *Bottom*) Normalized western band intensities.

It has been previously demonstrated that opened, damaged microtubules can be created by briefly exposing GMPCPP microtubules to calcium (33). Therefore, rhodamine-labeled GMPCPP microtubules were briefly incubated with 40 mM  $\text{CaCl}_2$ , and the  $\text{CaCl}_2$ -treated microtubules were imaged with TEM (Fig. 4C, *Top* and *SI Appendix*). From the TEM images, it was clear that portions of the GMPCPP microtubules were opened and/or damaged through the  $\text{CaCl}_2$  treatment (Fig. 4C, *Top*), which should allow increased access of  $\alpha\text{TAT1}$  to its acetylation site inside the microtubule lumen. Therefore, coverslip-adhered  $\text{CaCl}_2$ -treated microtubules were incubated with unlabeled  $\alpha\text{TAT1}$  in an imaging chamber for 30 min, and acetylation was then imaged with anti-acetylated tubulin antibody (Fig. 4C, *Bottom*). We found that  $\text{CaCl}_2$  treatment substantially increased both the number of patches per microtubule (Poisson regression,  $P < 2.2 \times 10^{-16}$ ) and the fraction of microtubules with patches (two-sample test of proportions,  $P < 2.2 \times 10^{-16}$ ) (Fig. 4D and *SI Appendix*, Fig. S4F).

To confirm that the antiacetylated tubulin antibody was properly reporting the acetylation of  $\text{CaCl}_2$ -treated microtubules, we performed a parallel experiment using western blots. Acetylated tubulin levels were measured over time for control and  $\text{CaCl}_2$ -treated microtubules (Fig. 4E, *Top* and *SI Appendix*, Fig. S4E), and the normalized band intensities were plotted as a function of  $\alpha\text{TAT1}$  incubation time (Fig. 4E, *Bottom*). We found that the  $\alpha\text{TAT1}$  acetylation level after 60–90 min of  $\alpha\text{TAT1}$  incubation time was 3.7-fold higher for  $\text{CaCl}_2$ -treated microtubules compared with control microtubules [Fig. 4E; green,  $\text{CaCl}_2$ ; red, controls (also plotted alone in *SI Appendix*, Fig. S1C); log-transformed linear regression,  $P = 0.003$ ], consistent with our fluorescence studies (Fig. 4D). In addition, we found that  $\alpha\text{TAT1}$  does not acetylate tubulin dimers as efficiently as it does intact microtubules, consistent with previous  $\alpha\text{TAT1}$  studies (18, 19) (Fig. 4E, blue).

Together, these results are consistent with the prediction that  $\alpha\text{TAT1}$  relies on microtubule ends and breaks or openings in the microtubule lattice to allow access to the lumen.

**$\alpha\text{TAT1}$  Exhibits Impeded Mobility Inside of the Microtubule Lumen.** Acetylation of stable microtubules may be limited both by  $\alpha\text{TAT1}$  entry into the lumen and by  $\alpha\text{TAT1}$  mobility within the lumen. To test  $\alpha\text{TAT1}$  mobility within the lumen, stabilized microtubules were incubated with  $\alpha\text{TAT1}$  for 5 or 120 min, and acetylation was visualized with fluorescently labeled antibody using TIRF microscopy as described above (Fig. 5A, *Left*). The overall increase in the fraction of acetylation per microtubule was then assessed by reporting the acetylation patch lengths on individual microtubules, normalized to microtubule length. We found that the fraction of acetylation per microtubule increased slightly but significantly when the  $\alpha\text{TAT1}$  incubation time was increased from 5 to 120 min (Fig. 5A, *Middle*). We found a similar small increase when the  $\alpha\text{TAT1}$  concentration was increased from 2.5 to 3.5  $\mu\text{M}$  (Fig. 5A, *Right*;  $\alpha\text{TAT1}$  incubation time of 30 min). This finding suggests that  $\alpha\text{TAT1}$  is able to acetylate new tubulin subunits continually within the lumen, but at a slow pace. The slow pace of acetylation may be due, in part, to slow diffusion of  $\alpha\text{TAT1}$  within the lumen, although, as previously reported (29), the presence of  $\alpha\text{TAT1}$  leads to slow microtubule depolymerization (*SI Appendix*, Figs. S2C and S4 C and D), which also likely causes preferential loss of acetylation patches at microtubule tips over time, leading to an underestimate of patch length growth over time.

Thus, to measure the mobility of  $\alpha\text{TAT1}$  within the microtubule lumen more directly, 15 nM  $\alpha\text{TAT1}$ -GFP protein was added to an imaging chamber with stabilized microtubules, and single-molecule movies were then collected using fast time-lapse TIRF microscopy (20 frames per second). We observed both slow- and fast-moving  $\alpha\text{TAT1}$ -GFP molecules (Fig. 5B, *Left*), which led to a wide range of measured diffusion coefficients (Fig. 5C, pink circles). We predicted that there may be a wide range of diffusion coefficients because, although many of the  $\alpha\text{TAT1}$ -GFP

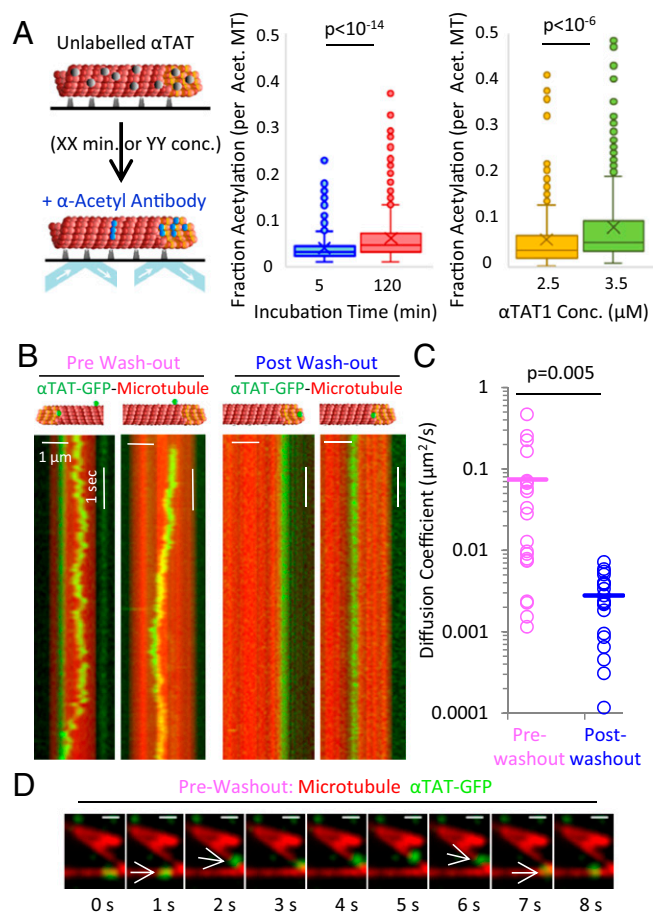


**Fig. 5.**  $\alpha\text{TAT1}$  exhibits slow mobility within the lumen. (A, *Left*) Schematic of acetylation TIRF experiment. (A, *Right*) Fraction of acetylated tubulin on acetylated microtubules with short and long  $\alpha\text{TAT1}$  incubation times (2.5  $\mu\text{M}$   $\alpha\text{TAT1}$ ) and low and high  $\alpha\text{TAT1}$  concentrations (30-min incubation), all normalized to individual microtubule lengths. In the plot, the first and third quartiles are at the ends of the box, the line in the center of the box is the median, the marker inside the box is the mean, and the markers outside of the box represent outliers above the first and third quartiles. Conc., concentration. (B) Kymographs of  $\alpha\text{TAT1}$  diffusion on GMPCPP microtubules before (*Left*) and after (*Right*) washout with buffer. (C) Diffusion coefficients for  $\alpha\text{TAT1}$ -GFP molecules imaged before (pink circles) or after (blue circles) washout. (D) Image panel from *Movie S3* of  $\alpha\text{TAT1}$ -GFP diffusion on microtubule lattice before washout. The white arrows pointing to an  $\alpha\text{TAT1}$ -GFP molecule jumping from one microtubule to another suggest external lattice diffusion. (Scale bars: 500 nm.)

molecules were bound to and diffusing on the outer lattice (16), some of the  $\alpha\text{TAT1}$ -GFP molecules could have entered the microtubule lumen; thus, these molecules would reflect the mobility of  $\alpha\text{TAT1}$ -GFP within the lumen. To evaluate the mobility of lumen-trapped  $\alpha\text{TAT1}$ -GFP, we incubated  $\alpha\text{TAT1}$ -GFP with coverslip-adhered microtubules and then washed the imaging chamber with warm buffer to remove the lattice-bound molecules, presumably leaving behind a portion of the lumen-trapped  $\alpha\text{TAT1}$ -GFP molecules. We then used fast time-lapse microscopy to collect movies of the microtubule-associated  $\alpha\text{TAT1}$ -GFP molecules that remained behind (Fig. 5B, *Right*). Importantly, we did not observe any fast-diffusing  $\alpha\text{TAT1}$ -GFP molecules after the washout, and, as a result, the postwashout diffusion coefficient for microtubule-associated  $\alpha\text{TAT1}$ -GFP molecules was over an order of magnitude smaller than the prewashout diffusion coefficient (Fig. 5C). This result suggests that after washout, the  $\alpha\text{TAT1}$ -GFP molecules that may have been trapped within the lumen remained behind, and that these molecules had limited

mobility, consistent with our fluorescent acetylation data and modeling work.

This result is in contrast to recent work by Szyk et al. (18), which suggested that luminal  $\alpha$ TAT1 was able to scan the length of the microtubule quickly. However, although our experimental prewashout measurements for the diffusion coefficient of  $\alpha$ TAT1 on the microtubule lattice were similar to the prewashout measurements reported by Szyk et al. (18),  $\alpha$ TAT1 has been reported to interact electrostatically with the outside of the microtubule lattice (16), and so we surmised that our prewashout diffusion coefficient largely reflected  $\alpha$ TAT1 diffusion on the outside of the microtubule. This argument is consistent with our observations of diffusing  $\alpha$ TAT1-GFP molecules “jumping” from one microtubule to another on the exterior surface of the microtubule in the prewashout movies (Fig. 5D and Movie S3).

#### Acetylated Patch Length Increases with Increasing Salt Concentration.

Our results are consistent with a model in which  $\alpha$ TAT1 exhibits slow and impeded mobility inside of the microtubule lumen. This slow and impeded mobility may be due to rapid rebinding of  $\alpha$ TAT1 to densely packed acetylation sites, as well as to a slow luminal  $\alpha$ TAT1 off-rate. Therefore, we reasoned that if the  $\alpha$ TAT1 rebinding rate was suppressed and the off-rate was increased, this net decrease in affinity for the  $\alpha$ TAT1 luminal acetylation site should lead to increased  $\alpha$ TAT1 mobility within the lumen, and subsequently to longer patches of microtubule acetylation. Consistent with this hypothesis, our simulations predicted that larger mean travel distances between rebinding events  $\langle \Delta x_{\text{lumen}} \rangle$  for luminal  $\alpha$ TAT1 molecules would lead to longer simulated acetylation patch lengths (Fig. 6A–C and SI Appendix).

To test this prediction, we noted that it has been previously demonstrated that the binding affinity of  $\alpha$ TAT1 for microtubules is suppressed at higher salt concentrations (16). Therefore, if the slow mobility of  $\alpha$ TAT1 inside of the microtubule lumen is due to rapid high-affinity binding to densely packed tubulin subunits, we predicted that by adding salt during  $\alpha$ TAT1 incubation, a net decrease in  $\alpha$ TAT1 affinity for the microtubule could lead to longer acetylation patch lengths. Thus, we performed the acetylation-TIRF experiments, but by adding different concentrations of KCl during  $\alpha$ TAT1 incubation. Strikingly, patch lengths were approximately threefold longer if the  $\alpha$ TAT1 incubation was carried out at high-salt conditions relative to our previous no-salt-added conditions (Fig. 6D and E; two-sample *t* test,  $P = 5.2 \times 10^{-12}$ ), whereas the size of  $\alpha$ TAT1 itself remained unchanged (Fig. 6E, Inset). This result supports a model in which the mobility of  $\alpha$ TAT1 within the microtubule lumen is controlled by its affinity to the densely packed acetylation sites within the lumen (Fig. 6F), and that reduced affinity in experiments with higher ionic strength allowed for increased mobility of  $\alpha$ TAT1 within the lumen.

Reduced  $\alpha$ TAT1 affinity for its acetylation binding site via increased ionic strength could explain, at least in part, the increased efficiency of  $\alpha$ TAT1 mobility in the experiments of Szyk et al. (18) compared with the data presented here. TIRF acetylation experiments in the report by Szyk et al. (18) were performed with 50 mM added KCl, which would be expected to increase acetylation patch lengths: as shown in Fig. 6E, we found that there was an approximately twofold increase in acetylation patch lengths with 50 mM added KCl compared with the “no-KCl-added” conditions in our baseline experiments.

#### Discussion

On the basis of our  $\alpha$ TAT1-GFP localization data, computational simulations, biochemical experiments, and acetylation localization data, we conclude that the foremost mode of entry for  $\alpha$ TAT1 into the microtubule lumen is through the microtubule ends, or through bends and breaks in the microtubule wall. This conclusion is in contrast to the model from Shida et al. (13), which suggested that  $\alpha$ TAT1 may access the microtubule lumen through regular lattice breathing at any position along the lattice,

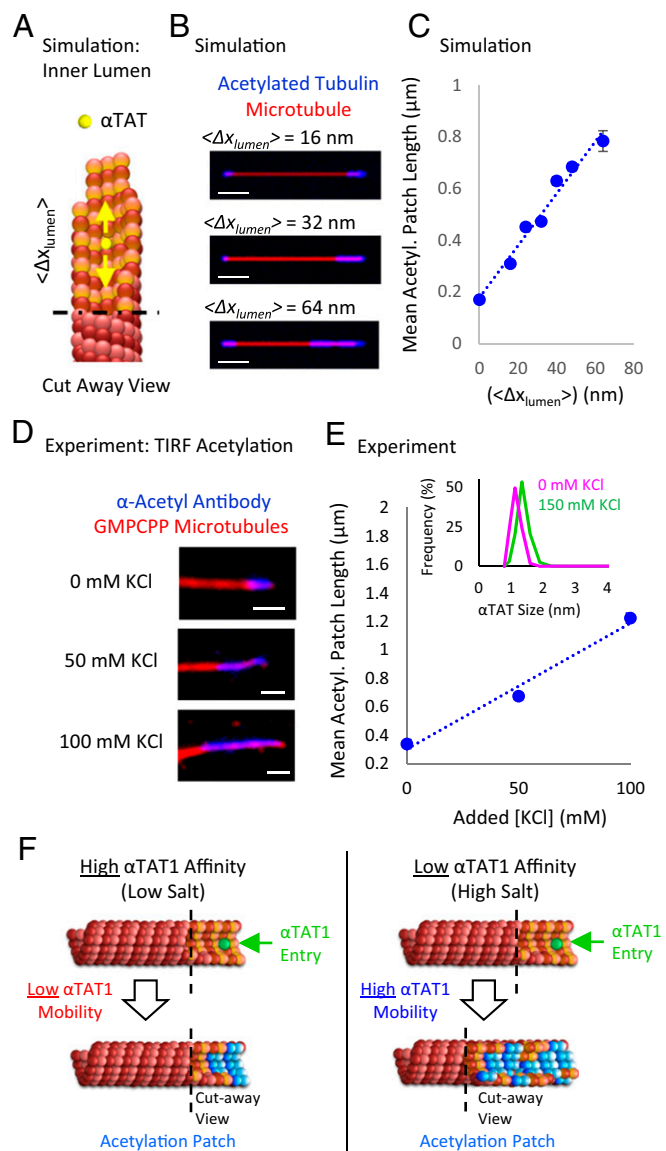


**Fig. 6.** Reduced binding affinity of  $\alpha$ TAT1 for microtubules leads to increased mobility within the lumen, and therefore increased acetylation patch lengths. (A) Schematic of  $\alpha$ TAT1 movement inside of the microtubule lumen. Yellow arrows represent the mobility of  $\alpha$ TAT1 within the lumen, which is described by the variable  $\langle \Delta x_{\text{lumen}} \rangle$ , the mean  $\alpha$ TAT1 travel distance between binding events. (B) Simulated TIRF microscopy images of acetylation patches with increasing  $\langle \Delta x_{\text{lumen}} \rangle$  for  $\alpha$ TAT1 (SI Appendix). (Scale bars: 1  $\mu\text{m}$ .) (C) Simulations predict that patch lengths will increase with increased travel distance between binding events for luminal  $\alpha$ TAT1 ( $\langle \Delta x_{\text{lumen}} \rangle$ ). (D) Example TIRF microscopy images from experiments with increasing added KCl concentration during  $\alpha$ TAT1 incubation. (Scale bars: 1  $\mu\text{m}$ .) (E) Patch lengths increase at higher KCl concentrations ( $n \geq 426$  each concentration, error bars 95% confidence intervals). (Inset)  $\alpha$ TAT1 Nanoflex size analysis (Materials and Methods), with (green line) and without (magenta line) added KCl. (F) Model for acetylation of stable microtubules in low (Left) and high (Right) salt.

but is consistent with findings from Akella et al. (12), in which the Lys40 acetylation signal formed a decreasing gradient that peaked at microtubule ends in axonemes. We also found that once  $\alpha$ TAT1 enters the microtubule lumen, it moves slowly down the lumen, and that this mobility is controlled by the affinity of  $\alpha$ TAT1 for the highly concentrated  $\alpha$ -tubulin acetylation sites within the lumen. This impeded mobility leads to concentrated patches of microtubule acetylation at the ends of stable microtubules.

Our results suggest that  $\alpha$ TAT1 enters the microtubule ends and preferentially acetylates these ends because  $\alpha$ TAT1 is not able to diffuse efficiently within the lumen. This conclusion is in contrast to recent work by Szyk et al. (18), which suggested that a high concentration of  $\alpha$ TAT1 was able to acetylate an entire microtubule almost simultaneously through longer acetylation bursts that occurred randomly along the microtubule length (18). Although one difference between our studies was in the ionic strength of the buffers, we also noted that a potentially important difference between the two studies was that we used GMPCPP-stabilized microtubules to analyze acetylation patterns on preformed microtubules, whereas Szyk et al. (18) used Taxol-stabilized microtubules. Both the timing and method of Taxol introduction have been shown to affect the structure of Taxol microtubules (34). Our work has demonstrated that microtubule structure, and particularly the presence of defects and openings in the microtubule lattice, would have a substantial impact on the efficiency of  $\alpha$ TAT1 in accessing and acetylating luminal acetylation sites. As shown in *SI Appendix, Fig. S5*, we found that one-step microtubule stabilization by Taxol may lead to more open, sheet-like microtubule structures, thus facilitating direct access of  $\alpha$ TAT1 to its acetylation site and potentially leading to a more dispersed acetylation pattern. Therefore, differences in the microtubule stabilization technique, in addition to the experimental ionic strength, may contribute to differing acetylation patterns between this study and the study of Szyk et al. (18).

Our results are consistent with a model in which  $\alpha$ TAT1 stochastically enters microtubule ends. Thus, if  $\alpha$ TAT1 never enters a microtubule end, the microtubule could remain unacetylated, even when nearby microtubules are partially or even fully acetylated. However, in stable cellular microtubule networks, where the  $t_{1/2}$  of some microtubules is  $\sim 2.2$  h (35), such as in neurons, it is more likely that  $\alpha$ TAT1 would ultimately enter the ends of a larger fraction of the microtubules, given their long lifetimes. Then,  $\alpha$ TAT1 may be able to acetylate the stable microtubules slowly while traveling down the lumen, especially under high-salt conditions such as is present inside of cells (Fig. 6F). In addition, we demonstrated that disruption of microtubule structure leads to an increase in microtubule acetylation (Figs. 3E and 4B–E), and that acetylation often occurs at breaks in the microtubule lattice (Fig. 4A), suggesting that microtubule bending and breaking may provide secondary  $\alpha$ TAT1 entry points to the lumen inside of cells. In cells, stable microtubule networks might naturally accumulate more lattice breaks

because of their long lifetimes, and so this enhanced accumulation could also contribute to an increase in overall acetylation of stable microtubule networks, as well as to the discontinuous staining of acetylated tubulin as has been observed in cells (21, 24, 25, 36, 37).

Other cellular influences may also have an impact on the efficiency of  $\alpha$ TAT1 acetylation in vivo. For instance, Kalebic et al. (29) found that  $\alpha$ TAT1 autoacetylation significantly increases the catalytic activity of  $\alpha$ TAT1. Autoacetylation of  $\alpha$ TAT1 could potentially increase the mobility of  $\alpha$ TAT1 within the lumen, perhaps by suppressing the binding affinity of  $\alpha$ TAT1 for its acetylation site. Additionally, Montagnac et al. (38) found that clathrin-coated pits localize  $\alpha$ TAT1 to the ends of growing microtubules, which would subsequently increase the opportunity for  $\alpha$ TAT1 to enter the lumen. This  $\alpha$ TAT1 localization led to stretches of acetylation near to the microtubule end, similar to what we observed in our in vitro studies. Thus, factors that localize  $\alpha$ TAT1 to microtubule plus-ends could also increase the efficiency of  $\alpha$ TAT1 acetylation in vivo.

In summary, our data support a model in which  $\alpha$ TAT1 stochastically enters the lumen at microtubule ends, or through breaks in the lattice. Then, the mobility of  $\alpha$ TAT1 within the lumen is controlled by the affinity of  $\alpha$ TAT1 for its binding sites, which are highly concentrated within the lumen. Important future efforts will involve identifying regulators of  $\alpha$ TAT1 that could facilitate its end-entry and luminal mobility, as well as studies to determine whether  $\alpha$ TAT1 itself could potentially modulate microtubule dynamics to allow access to the lumen.

## Materials and Methods

**Experimental.**  $\alpha$ TAT1 proteins were expressed in *Escherichia coli* cells, and the interactions with reconstituted microtubules were then visualized using either TIRF microscopy or western blots as described in *SI Appendix*.

**Simulation.** Simulation code was written in MATLAB (MathWorks), and then run on personal computers as described in *SI Appendix*.

**ACKNOWLEDGMENTS.** We thank Brandon Coombes for statistical analysis assistance. This work was funded by an American Heart Association Predoctoral Fellowship (to C.C.). This work was supported by the Pew Charitable Trusts through the Pew Scholars Program in the Biomedical Sciences (M.K.G.) and by NIH National Institute of General Medical Sciences Grant GM-103833 (to M.K.G.). Parts of this work were carried out in the Characterization Facility, University of Minnesota, a member of the National Science Foundation-funded Materials Research Facilities Network ([www.mrfn.org](http://www.mrfn.org)) via the Materials Research Science and Engineering Centers program.

- Quinones GB, Danowski BA, Devaraj A, Singh V, Ligon LA (2011) The posttranslational modification of tubulin undergoes a switch from deetyrosination to acetylation as epithelial cells become polarized. *Mol Biol Cell* 22(7):1045–1057.
- Janke C, Bulinski JC (2011) Post-translational regulation of the microtubule cytoskeleton: Mechanisms and functions. *Nat Rev Mol Cell Biol* 12(12):773–786.
- Soppina V, Herbstman JF, Skiniotis G, Verhey KJ (2012) Luminal localization of  $\alpha$ -tubulin K40 acetylation by cryo-EM analysis of fab-labeled microtubules. *PLoS One* 7(10):e48204.
- Nogales E, Whittaker M, Milligan RA, Downing KH (1999) High-resolution model of the microtubule. *Cell* 96(1):79–88.
- Arce CA, Casale CH, Barra HS (2008) Submembrane microtubule cytoskeleton: Regulation of ATPases by interaction with acetylated tubulin. *FEBS J* 275(19):4664–4674.
- Wickström SA, Masoumi KC, Khochin S, Fässler R, Massoumi R (2010) CYLD negatively regulates cell-cycle progression by inactivating HDAC6 and increasing the levels of acetylated tubulin. *EMBO J* 29(1):131–144.
- Castro-Castro A, Janke C, Montagnac G, Paul-Gilloteaux P, Chavrier P (2012) ATAT1/MEC-17 acetyltransferase and HDAC6 deacetylase control a balance of acetylation of alpha-tubulin and cortactin and regulate MT1-MMP trafficking and breast tumor cell invasion. *Eur J Cell Biol* 91(11–12):950–960.
- Hempfen B, Brion JP (1996) Reduction of acetylated alpha-tubulin immunoreactivity in neurofibrillary tangle-bearing neurons in Alzheimer's disease. *J Neuropathol Exp Neurol* 55(9):964–972.
- Outeiro TF, et al. (2007) Sirtuin 2 inhibitors rescue  $\alpha$ -synuclein-mediated toxicity in models of Parkinson's disease. *Science* 317(5837):516–519.
- Godena VK, et al. (2014) Increasing microtubule acetylation rescues axonal transport and locomotor deficits caused by LRRK2 Roc-COR domain mutations. *Nat Commun* 5:5245.
- Dompierre JP, et al. (2007) Histone deacetylase 6 inhibition compensates for the transport deficit in Huntington's disease by increasing tubulin acetylation. *J Neurosci* 27(13):3571–3583.
- Akella JS, et al. (2010) MEC-17 is an alpha-tubulin acetyltransferase. *Nature* 467(7312):218–222.
- Shida T, Cueva JG, Xu Z, Goodman MB, Nachury MV (2010) The major alpha-tubulin K40 acetyltransferase alphaTAT1 promotes rapid cilogenesis and efficient mechanosensation. *Proc Natl Acad Sci USA* 107(50):21517–21522.
- Kalebic N, et al. (2013)  $\alpha$ TAT1 is the major  $\alpha$ -tubulin acetyltransferase in mice. *Nat Commun* 4:1962.
- Perdiz D, Mackeh R, Poüs C, Baillet A (2011) The ins and outs of tubulin acetylation: More than just a post-translational modification? *Cell Signal* 23(5):763–771.
- Howes SC, Alushin GM, Shida T, Nachury MV, Nogales E (2014) Effects of tubulin acetylation and tubulin acetyltransferase binding on microtubule structure. *Mol Biol Cell* 25(2):257–266.
- Yajima H, et al. (2012) Conformational changes in tubulin in GMPCPP and GDP-taxol microtubules observed by cryoelectron microscopy. *J Cell Biol* 198(3):315–322.
- Szyk A, et al. (2014) Molecular basis for age-dependent microtubule acetylation by tubulin acetyltransferase. *Cell* 157(6):1405–1415.
- Maruta H, Greer K, Rosenbaum JL (1986) The acetylation of alpha-tubulin and its relationship to the assembly and disassembly of microtubules. *J Cell Biol* 103(2):571–579.
- Kormendi V, Szyk A, Piszczek G, Roll-Mecak A (2012) Crystal structures of tubulin acetyltransferase reveal a conserved catalytic core and the plasticity of the essential N terminus. *J Biol Chem* 287(50):41569–41575.
- Piperno G, LeDizet M, Chang XJ (1987) Microtubules containing acetylated alpha-tubulin in mammalian cells in culture. *J Cell Biol* 104(2):289–302.

